

Soft Optical Sensor and Haptic Feedback System for Remote and Robot-Assisted Palpation

Arincheyan Gerald¹, Jonathan Ye¹, Rukaiya Batliwala¹, Patra Hsu², Johann Pang² and Sheila Russo^{1,3,4}

Abstract—Robotic palpation shows significant potential to improve the accuracy and speed of tumor identification. However, robotic palpation mechanisms often lack haptic feedback, making it difficult for the surgeon to identify variations in tissue stiffness. This paper presents a soft optical sensor integrated with a wearable haptic glove for tumor detection during robotic palpation. The sensor contains an array of optical waveguides that can detect the presence of tumors embedded within a tissue phantom. Detection of a tumor results in an optical loss from the waveguide signal, triggering proportional inflation of the soft microfluidic actuators in the glove. The glove consists of four modular actuators placed at the fingertips, each corresponding to a sensing location on the waveguide array. The inflation of each actuator is proportional to the incident loss on the palpation sensor array, which is dependent on tumor depth. Thus, the glove is capable of alerting the user to the location of tumors during remote palpation.

I. INTRODUCTION

With the growing adoption of minimally invasive surgical procedures across medical fields, robotic and remote palpation of tissue is becoming more commonplace [1], [2]. Robotic palpation can serve as an effective alternative to manual palpation, by potentially providing higher accuracy of tumor detection and reduced application of forces [3]. This can reduce the time required for the identification of conditions such as cancer and other abnormalities [4]. However, unlike manual palpation, robotic palpation is performed by an end-effector and does not allow the surgeon to directly feel the tissue. Thus, the end effector must be sensorized to quantify the variability in stiffness to identify tumors and other abnormalities [5]. Despite the sensorization of the end effector, the surgeon still cannot directly feel the transmission of forces and distinction of tissue stiffness. Additionally, the lack of tactile feedback is further exacerbated in cases of remote palpation, as the surgeon may not be physically present in the operating room and must

*This work was supported by the National Institute of Biomedical Imaging and Bioengineering of the National Institutes of Health under award number R21EB029154, by the the National Center for Advancing Translational Sciences, National Institutes of Health, through BU-CTSI Grant Number 1UL1TR001430, and by the Boston University Undergraduate Research Opportunities Program. Its contents are solely the responsibility of the authors and do not necessarily represent the official views of the NIH.

¹A. Gerald, R. Batliwala, J. Ye and S. Russo (corresponding author) are with the Mechanical Engineering Department, Boston University, Boston, MA 02215 USA.

²P. Hsu and J. Pang are with the Biomedical Engineering Department, Boston University, Boston, MA 02215 USA .

³S. Russo is with the Center for Information and Systems Engineering, Boston University, Boston, MA 02215 USA.

⁴S. Russo is with the Materials Science and Engineering Division, Boston University, Boston, MA 02215 USA.

E-mail: russos@bu.edu.

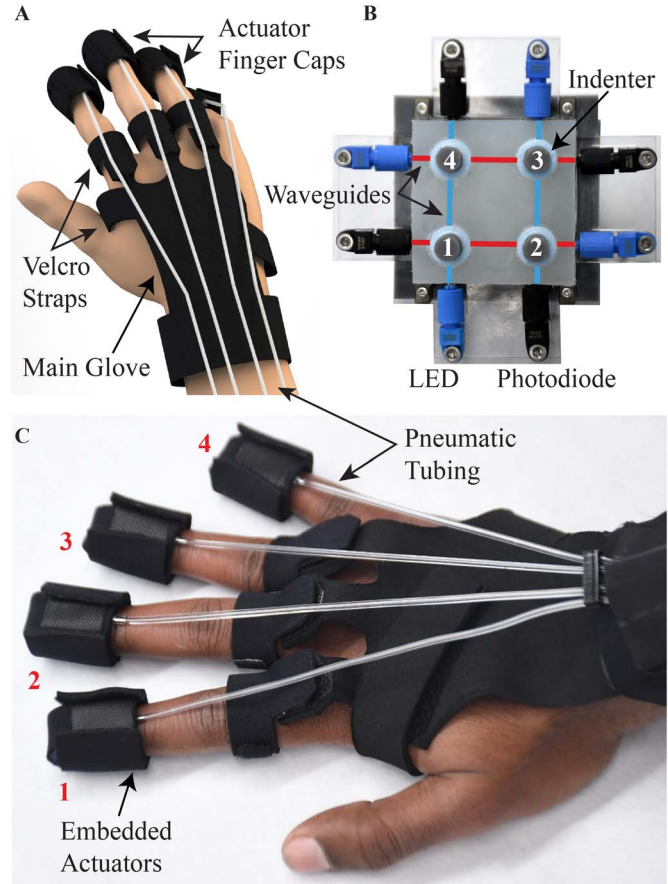


Fig. 1. Proposed system for remote and robot-assisted palpation: soft optical palpation sensor and wearable haptic glove. A) 3D rendering of the wearable haptic glove with labelled components. B) Soft optical palpation sensor with top waveguide layer highlighted in blue and bottom waveguide layer highlighted in red and corresponding detection points where the waveguides intersect. C) Image of wearable haptic glove showing numbered actuators on fingertip corresponding to detection points on the soft optical palpation sensor.

rely purely on teleoperation [6], [7]. Thus, there is a crucial need to restore tactile sensation to the surgeon's hand so that they are able to discern tissue and force interactions during the procedure [8]. Haptic feedback combined with sensing can improve performance and increase the intuitiveness and efficiency of robotic palpation [9], [10]. However, there are challenges present in restoring feedback to the surgeon, including choosing the optimal method of sensory feedback, avoiding distracting the surgeon with an overload of sensory information, and ensuring the device does not impede the clinical workflow [11]–[14]. Feedback to the surgeon in such cases is often provided through sensory substitution, i.e., the replacement of direct haptic forces with vibrotactile feedback

or audiovisual methods, which affects the intuitiveness of the procedure [6], [9].

Previous works have attempted to eliminate sensory substitution by providing direct pneumatic haptic feedback via soft actuators that inflate to press against the user's fingertip. However, these solutions present ergonomic limitations, such as bulkiness or require the user to continuously hold or pinch the device with their fingertips, thereby constraining the free movement of the user's hands [15]–[17]. Furthermore, most pneumatic haptic systems provide only single-point feedback, making it harder to convey the localization of features and tumors within a given palpation region [15]. Additionally, non-pneumatic haptic feedback solutions often utilize expensive and complex rigid mechanisms to generate forces against the fingertip [18], [19]. Thus, there is a need for a multi-finger direct haptic feedback system that is ergonomic, soft and cost-effective.

Similarly, palpation sensors often consist of rigid probes and linear mechanisms, which may pose difficulties as they require existing instruments to be modified [5], [9], [20]. Palpation sensors have also utilized piezoresistive and capacitive technologies but suffer from biocompatibility issues and noise [21]. Soft optical sensors have also been widely used due to their passive and biocompatible nature along with their small size [21]. However, many optical palpation sensors use expensive electronic equipment such as imaging cameras and fiber Bragg gratings [22], [23] and require complex manufacturing techniques. Due to the cost and complexity of their components, optical palpation sensors usually are not disposable after each palpation procedure and must be sterilized [24].

This paper presents a low-cost and easy to fabricate soft optical sensor and haptic feedback system for remote and robot-assisted palpation (Fig. 1). The soft optical sensor can detect the location of tumors embedded in a tissue phantom via monitoring the change in optical signal during palpation (Fig. 1, B). The sensor output connects to a wearable haptic glove equipped with multi-finger silicone actuators that inflate upon tumor detection (Fig. 1, A, C). The soft optical sensor is made from readily available materials, using tubing as optical waveguides immersed in soft silicone elastomer. This allows the sensor to be rapidly fabricated and disposed of after use. The actuators provide combined cutaneous pneumatic and vibrotactile feedback. The wearable glove is lightweight, has a low profile and the actuators wrap around the user's fingertips in an ergonomic manner (Fig. 2, A-D). The actuators are easy to fabricate and can be easily disposed of after use, if needed.

II. MATERIALS AND METHODS

This section describes the soft palpation sensor and haptic feedback glove design, fabrication, as well as the fluidic control circuit and pulse-width modulation (PWM) control strategy.

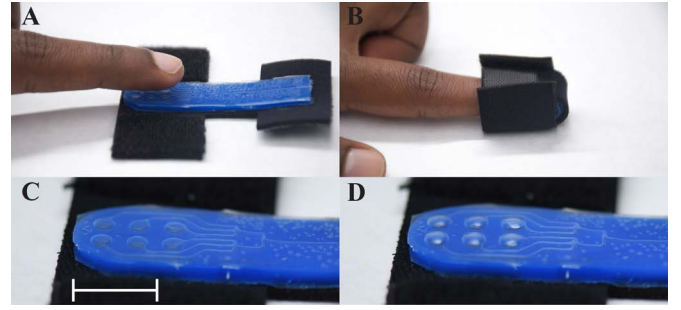


Fig. 2. Soft robotic actuators embedded in the wearable haptic glove. A) Image showing actuator and fabric straps in an unwrapped configuration. B) Image showing actuator and fabric straps wrapped around the finger. C) Deflated microfluidic actuator. D) Inflated microfluidic actuator with embedded pneumatic channels visible. Scale bar measures 1 cm.

A. Haptic Palpation System Design

1) *Palpation Sensor Design:* The soft optical palpation sensor consists of a simple, easy to fabricate design utilizing readily available materials such as PVC tubing as optical waveguides and soft silicone elastomer. The sensor can be manufactured rapidly (see Section II-B.1) and at a low cost. This allows it to be removed from the robotic end effector between procedures and disposed of, if necessary. Furthermore, the inertness of the optical sensor makes it inherently safe for palpation. There is no voltage or current inside the sensing apparatus nor is there any heat or magnetic fields. As seen in Fig. 1 B, the sensor consists of four clear PVC tubes that serve as waveguides. The optical clarity of the tubing is conducive to the transmission of light. The tubes are arranged in two layers, consisting of two waveguides each. The bottom and top waveguides form a lattice-shaped array encased within a soft silicone cladding (Ecoflex 00-50, Smooth-On Inc.), see Fig. 1 B and Fig. 3 F. Rigid indenters are attached to the soft silicone cladding beneath the four locations where the waveguides intersect each other (Fig. 1 B). The indenters serve as detection points to enable effective palpation of tissue and translate any incident force from tumors onto the waveguides. The transmission of light through the waveguides can be recorded as a voltage using the optoelectronic circuit described in Section II-C. The presence of a hard tumor within the tissue phantom will cause a higher measured optical loss (reduction in light transmission) at the detection points when compared to palpating the tumor-less phantom. The waveguides in the bottom layer are most sensitive to deformation due to their proximity to the top of the indenters (Fig. 1. B). This layer exhibits higher optical losses upon pressing against a tumor. The waveguides in the upper layer are further removed from the indenters (due to the silicone cladding) and thus exhibit a lower loss. Consequently, the bottom layer of the sensor is used to estimate the tumor depth (i.e., magnitude of optical loss) whereas the top layer of the sensor is used to locate and triangulate the tumor. This allows the user to locate the presence of the tumor at the four detection points (Fig. 1. B). The sensor measures $51\text{ mm} \times 51\text{ mm}$ and each detection point is 27 mm apart. The silicone cladding is 5.7 mm thick, with the attached indenters protruding 10 mm. The sensor is

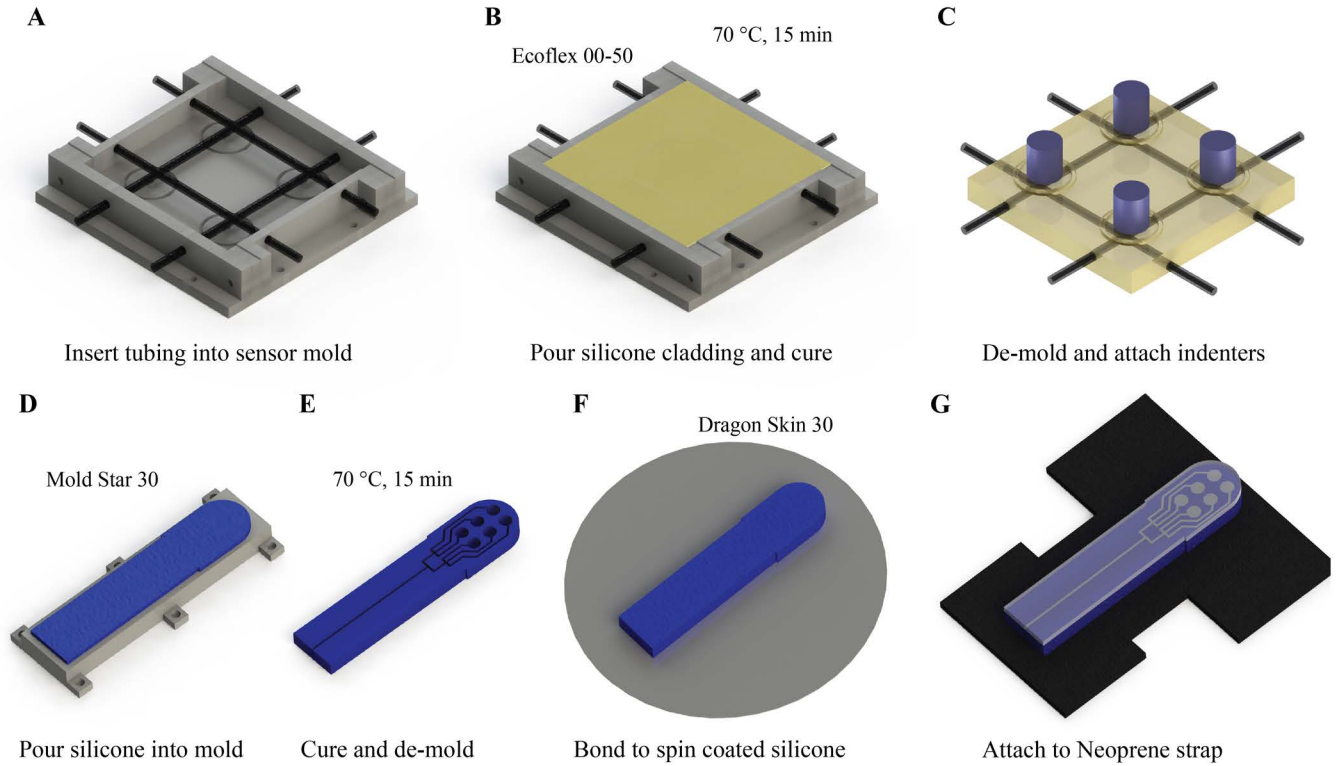


Fig. 3. *Top* - Soft Optical Palpation Sensor Fabrication. A) Align tubes within 3D printed mold. B) Pour silicone elastomer into mold and cure. C) De-mold sensor and attach indenters. *Bottom*- Actuator Fabrication for the wearable haptic glove. D) Pour silicone into actuator base mold. E) Heat cure and de-mold actuator base after curing. F) Spin coat silicone membrane onto silicon wafer and bond actuator base. G) Cut out the silicone actuator and glue to fabric straps.

attached to a 3D printed holder that allows the device to be attached onto a robotic end effector.

2) *Haptic Glove Design*: The wearable robotic glove consists of four pneumatic actuators connected to a main glove piece that guides pneumatic tubing along the user's hand (Fig. 1, C). The glove is designed to be lightweight and modular, thereby being able to fit a variety of hand sizes using adjustable Velcro straps. The pneumatic actuators are composed of microfluidic arrays made of a silicone base with a thin silicone membrane at the top (Fig. 2, A-D). The actuators inflate upon detection of an incident loss (tumor), pressing and vibrating against the user's fingertips at 20 Hz via a PWM control algorithm. This provides a combined sensation of direct pneumatic feedback and vibrotactile feedback to alert the user to the presence of a tumor. Each of the four actuators on the glove map to a specific detection point on the palpation sensor. For example, when a tumor is located at the indenter detection point (Fig. 1, B), i.e., the intersection of one bottom layer and top layer waveguide, then the corresponding actuator inflates in proportion to the optical loss. The actuators are placed sequentially on the fingertips instead of a matrix on another area of the hand primarily due to the sensitivity of the fingertips to haptic feedback compared to other areas of the hand. If the resolution of the sensor were to increase, the number of actuators on the fingertips would correspondingly increase as well. The actuator straps and the main glove are made from 1.5 mm thick neoprene (SewSwank) thereby proving

a lightweight design and low vertical profile. The actuators and the main glove piece can be fabricated rapidly at a low cost due to the nature of materials used (see Section II-B.2). This means the glove and its actuators can be easily disposed of, if necessary (e.g., if the glove becomes contaminated or dirty).

B. Fabrication

1) *Palpation Sensor Fabrication*: The optical waveguides consist of clear PVC tubing (2 mm OD, 60A durometer, McMaster-Carr Supply Company). The tubing is cut into 8 cm lengths and arranged symmetrically in a lattice-shaped 3D printed mold (Form 2, Formlabs) (Fig. 3, A). The tubing is temporarily reinforced with 0.38 mm steel rods (McMaster-Carr Supply Company) to prevent deformation during the silicone curing process. Ecoflex 00-50 silicone is then poured into the mold and cured at 70° C for 15 min (Fig. 3, B). The metal rods are removed after the sensor is fully cured. The cladding and tubing waveguides are then de-molded and attached to a flat acrylic backing (1.3 mm in thickness, McMaster-Carr). 3D printed indenters (Form 2, Formlabs) are then attached to the cladding using silicone rings (Smooth-Sil 950, Smooth-On Inc.) and flexible adhesive (Loctite 4861) (Fig. 3, C). The sensor is then mounted onto a 3D printed holder that can attach onto a robotic end effector. The total fabrication time for the sensor is ≈ 60 min.

2) *Haptic Glove Fabrication*: The base of the microfluidic actuators on the glove are fabricated by pouring silicone elastomer (Mold Star 30, Smooth-On Inc) into patterned 3D

printed molds (Form 2, Formlabs) (Fig. 3, D). The silicone in the mold is then cured at 70° C for 15 min (Fig. 3, E). Dragon Skin 30 (Smooth-On Inc) silicone elastomer is then spin coated onto a silicon wafer (5 s ramp, 40 s dwell, 500 rpm) to form a 300 μm thin layer. The Dragon Skin 30 layer is cured for 10 minutes at 70° C. This serves as the top membrane of the actuator. A thin layer of Ecoflex 00-30 (Smooth-On Inc.) is spin coated (5 s ramp, 30 s dwell, 1000 rpm) onto the silicone coated wafer. The Ecoflex serves as a flexible glue to bond the actuator base onto the top Dragon Skin 30 membrane. The actuator base is then pressed onto the wafer and cured at 70° C for 5 min (Fig. 3, F). The actuator is cut into shape and glued to the 1.5 mm Neoprene fabric straps (Fig. 3, G). The main glove piece is also cut from Neoprene and Velcro straps are attached. Finally, tubing (2 mm OD, McMaster-Carr Supply Company) is inserted into the actuators to form the completed glove. The actuator design allows it to fold around the fingertips using Velcro straps. This provides a secure fit and direct contact between the microfluidic actuator array and finger pads. The total fabrication time is ≈30 min. Please refer to the accompanying video for additional information.

C. Control

The four microfluidic actuators on the haptic glove are pneumatically controlled by four solenoid valves that are attached to a manifold (GVP-321C-24D, Nitra® Pneumatics). The on/off switching of the solenoid valves is controlled by a multi-channel MOSFET module (Hilitand). The MOSFET module is in turn connected to an Arduino® Mega 2560 micro-controller. The control strategy for the palpation system uses pulse width modulation (PWM) to set the duty cycle controlling the solenoid valves based on the palpation sensor input during robotic palpation (Fig. 4). Thus, the magnitude of the optical loss caused by the tumors (i.e., incident force on the sensor's indenters) determines the value of the duty cycle. This in turn triggers proportional inflation of the pneumatic actuators to alert the user of the presence of the tumor.

The duty cycle equation can be calibrated depending on the type of robotic palpation i.e., tumor hardness and indentation depth. The general duty cycle equation is as follows:

$$\text{Duty Cycle [\%]} = \text{Optical Loss (dB)} \times T \quad (1)$$

The duty cycle is calculated by multiplying the *Optical Loss (dB)* by a constant *T*. The constant can be set so that the duty cycle triggers inflation of the actuators when the optical loss crosses an threshold value and reaches 100% when the optical loss from tumor palpation saturates at its highest value. The threshold and saturation values of the optical loss are ultimately dependent on the specific palpation procedure and tumor hardness. Thus they can be calibrated as needed. The optical loss is calculated using the following formula:

$$\text{Loss (dB)} = 10 \times \log_{10}(I_0/I) \quad (2)$$

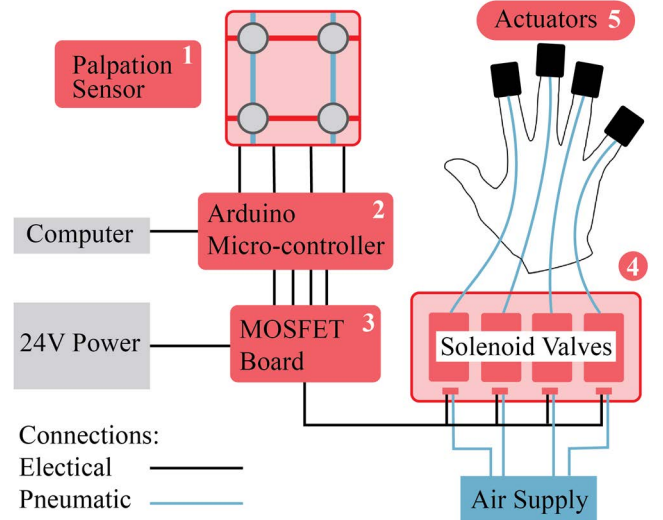


Fig. 4. Block diagram showing control circuit. 1) Palpation sensor. 2) Arduino. 3) 4-channel MOSFET board. 4) Solenoid valves. 5) Microfluidic actuators.

where I_0 is the output power of the undeformed tubing waveguide on the soft palpation sensor when it is not pressing on any tissue, and I is the power through the waveguide when the sensor is deformed due to the incident force caused by pressing the tissue phantom. The change in output power I is measured as a change in voltage recorded by the optoelectronic circuit. The circuit consists of four 930 nm, infrared LEDs (IF E91-A, Industrial Fiber Optics) that emit light through the waveguides connected to four photo-transistors (IF D92, Industrial Fiber Optics). Please refer to the accompanying video for additional information.

III. RESULTS AND DISCUSSION

This section describes the experiments performed in this work to validate the soft palpation sensor and haptic feedback glove. This includes actuator characterization tests, i.e., the PWM duty cycle vs pressure validation and blocked force testing, as well as sensor characterizations, i.e., the tumor depth estimation and *in-vitro* evaluation.

A. Pressure Holding Validation

The microfluidic actuators on the glove were subjected to periodic and incremental changes in the input duty cycle. In response to changes in the duty cycle, the actuators inflated proportionally and the corresponding pressure was measured using a pressure transducer (BSP000W, Balluf Inc.). This test was performed to evaluate the ability of the microfluidic actuators to hold distinct and discernable pressure values as the input loss from the palpation sensor increases during palpation of tumors at different depths. This is necessary as the surgeon must be able to feel the approximate depth of the tumor during the palpation process i.e., a tumor near the surface of the tissue will cause greater inflation of the actuators (pressure) compared to a deeper tissue. As seen in Fig. 5, the duty cycle increases in 10% increments from 0 to 100% at a PWM frequency of 20 Hz. The corresponding pressure in the actuators increases linearly starting from 30%

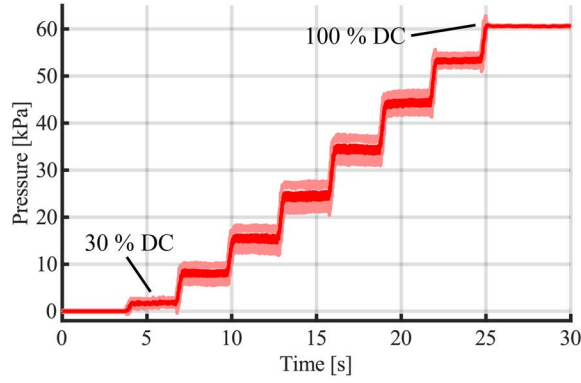


Fig. 5. Test results displaying periodic increase in microfluidic actuator pressure as the duty cycle is increased by 10% increments.

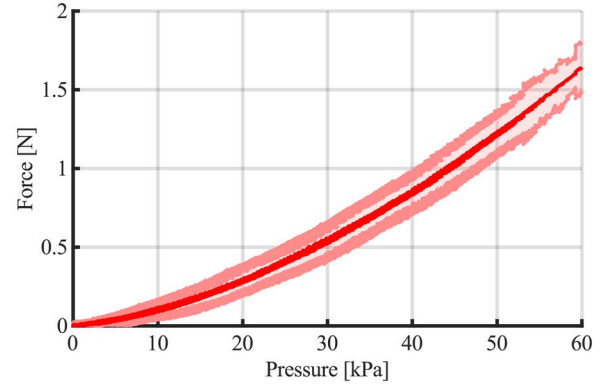


Fig. 6. Test results displaying blocked force in response to actuator inflation.

of the duty cycle value to 100% to a max pressure of 60 kPa. The actuators do not inflate at duty cycle values below 30% as the time fraction of the cycle during which the solenoids are open is too short to cause sustained inflation of the actuators. Additionally, the graph shows oscillating pressure values at each duty cycle step, this is due to the PWM control of the solenoids causing the actuator membrane to vibrate. This is perceived by the user as a combined vibrotactile and pneumatic feedback. At higher values of the duty cycle, the vibration from the oscillating pressure decreases and pneumatic feedback begins to dominate.

B. Blocked Force Testing

Blocked force testing was performed in order to quantify the magnitude of force that the actuators exert upon complete inflation. The microfluidic actuators were placed underneath a compression anvil that was fastened to a load cell (2580, Instron Corp.) connected to an Instron table frame (5943, Instron Corp.). The PWM duty cycle increased linearly such that the actuator reached full inflation at 60 kPa. As seen in Fig. 6, the force increase from 0 N to an average value of 1.6 N as the pressure reaches 60 kPa. The rate of change of the blocked forces increases faster as the pressure reaches the upper values of 40-60 kPa. While the blocked force testing anvil may not mimic the soft and deformable nature of the fingertip, it provides an estimate of the force behaviour of the actuator in response to changes in the stimuli (loss from palpation).

C. Tumor Detection and Localization

This test was conducted to assess the ability of the soft palpation sensor to detect tumors at varying depths within a tissue phantom. In order to localize the tumor, the sensor must be able to estimate the depth of the tumor underneath the phantom, in addition to its location in the X-Y plane on the surface of the palpated tissue. A 16 mm thick tissue phantom was fabricated out of Ecoflex 00-10 (10 shore 00 hardness, Smooth-On Inc.). The tissue phantom contained four embedded spherical tumors of 50A shore hardness (Smooth-Sil 950, Smooth-On Inc.). The 10 mm diameter

tumors were embedded at depths ranging from 2 mm to 5 mm beneath the tissue surface. The palpation sensor was mounted onto an Instron frame (5943, Instron Corp.). The sensor was then pressed onto the tissue phantom to a depth of 8 mm and rate of 2 mm/s to simulate palpation. Each detection point was pressed onto the four tumor locations and the subsequent loss was recorded. As seen in Fig. 7, both the bottom layer and top layer waveguides show a sustained increase in optical loss when pressing on a location with a tumor compared to the tumor free location. As the tumor depth increases, the loss experience by the waveguides decreases linearly. The bottom waveguides are more sensitive to the presence of the tumor, showing an average optical loss ranging from 4.5 dB to 3.2 dB as depth increases from 2 mm to 5 mm. The baseline average loss of the bottom layer when there is no tumor is 1.3 dB. The top waveguide layer is less sensitive to the tumor but it also shows distinct loss when palpating a tumor. The loss ranges from 1.5 dB to 1 dB from tumor depths ranging from 2 to 5 mm. The baseline average loss when there is no tumor is 0.2 dB. Thus, the sensor is able to distinguish the presence of a tumor and its location, as the resultant loss is significantly higher than the baseline loss when palpating only the tissue phantom.

D. In-Vitro Validation

An *in-vitro* validation of the soft optical palpation sensor and wearable haptic glove was conducted to evaluate the performance of the system in a clinical setting i.e., a robotic palpation test. The palpation sensor was mounted onto a UR-5 robotic arm (Universal Robots) and placed directly above a tissue phantom (00-10 shore hardness) with embedded tumors of 50 A shore hardness (Fig. 8). First, the robot arm presses directly into the tissue phantom at the center, where there are no embedded tumors. The arm palpates the tissue at a rate of 1 mm/s to a final depth of 8 mm. The robot arm then moves up from the surface and moves the sensor to a tumor location that is 15 mm along the x-axis and 15 mm away on the y-axis from the defined center origin. Herein lies a tumor embedded 3 mm below the surface. The arm then presses the sensor into the tissue phantom at the same rate

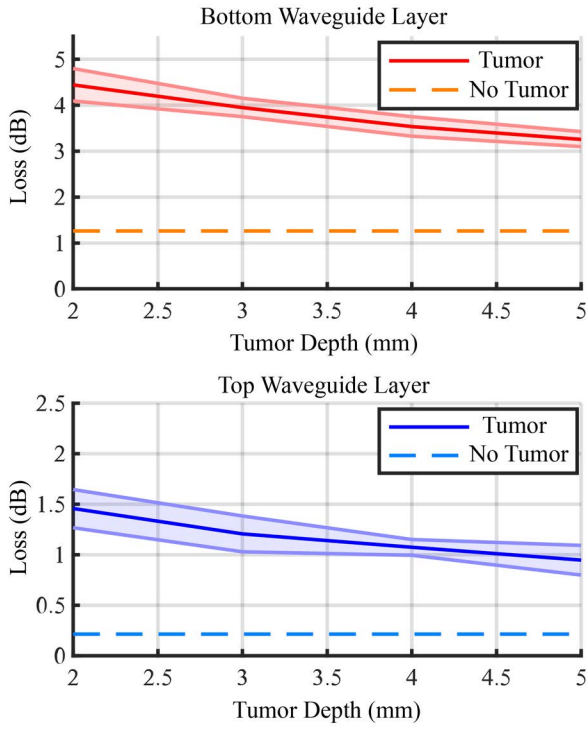


Fig. 7. Test results displaying average optical loss of the sensor in response to palpating tumors embedded at varying depths for 50A shore hardness tumors. The dotted lines show the mean loss for the top and bottom waveguide layers when there is no tumor in the phantom.

and depth as previously mentioned. As seen in Fig. 9, when the sensor is pressed on the phantom with no tumors (10 s to 40 s in Fig. 9), the bottom two waveguides that are closest to the indenters show the same loss of 1.5 dB, which is beneath the set tumor detection threshold for the bottom layer. The top waveguide layers show differing losses, with the top waveguide 1 showing approximately 0.5 dB loss while the second top waveguide shows 0.1 dB loss. However, both waveguides are below the set tumor detection threshold for the top layer. The robotic arm then moves the sensor to the next location, where the palpation motion is performed again. As the sensor presses against the embedded tumor (70 s to 85 s in Fig. 9), the loss from the first waveguide in the bottom layer increases beyond the threshold loss value and reaches 3.5 dB. Concurrently, the loss from the first waveguide in the top layer also increases beyond the set loss threshold value. Using the loss signal from the two waveguides, the position of the tumor can be localized to detection point 1, i.e., the position above the first indenter where the bottom waveguide 1 and top waveguide 1 intersect in a lattice. Consequently, the microfluidic actuator on the glove corresponding to the detection point inflates. Upon tumor detection, the duty cycle value of the actuators rises to around 70% and stays constant as the sensor is pressed against the tumor. Once, the sensor completes the palpation process and rises up, the duty cycle drops as well. Please refer to the accompanying video for additional information. In future works, the haptic glove will be evaluated through user trials. This would assess how haptic feedback could improve tumor detection during the

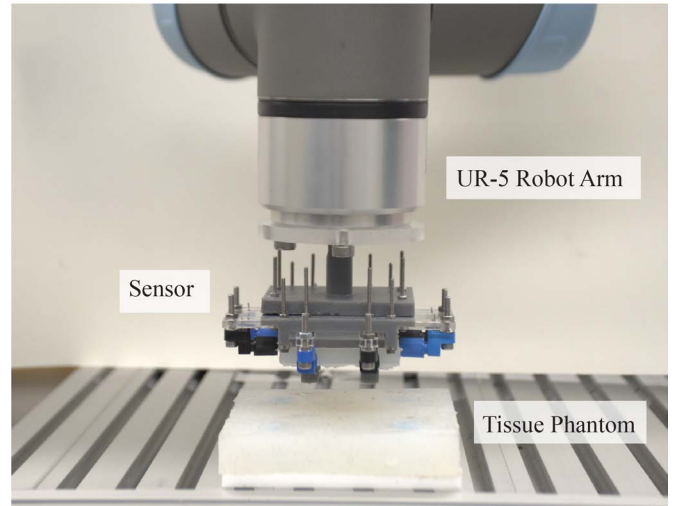


Fig. 8. *In-vitro* validation test setup showing the soft optical palpation sensor, UR-5 robot arm, and tissue phantom with embedded tumors

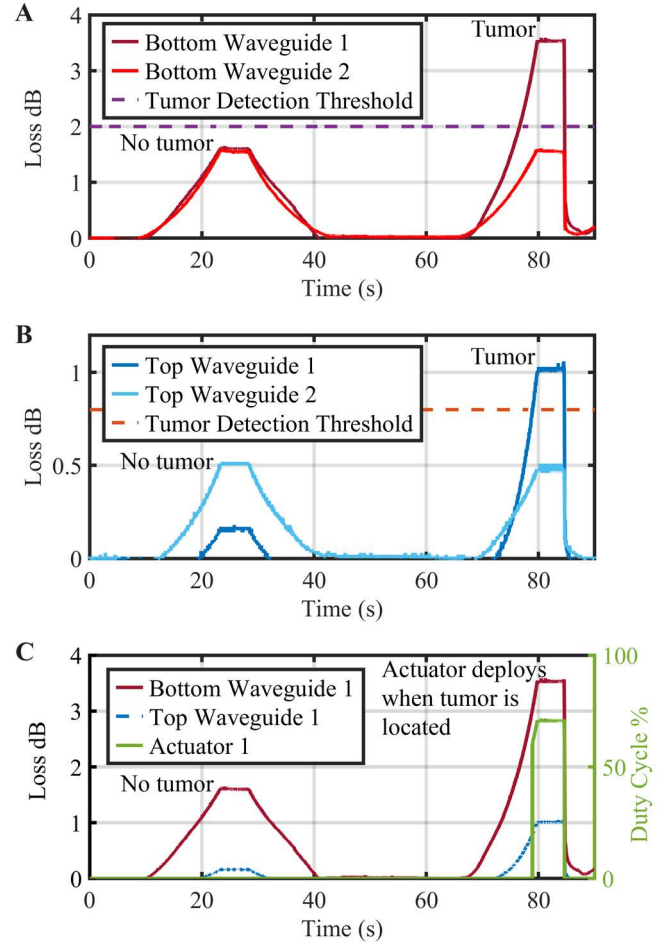


Fig. 9. Figure showing the loss signals of the sensor and duty cycle data during the *in-vitro* palpation test. A) Loss of the bottom two waveguides when pressing against the tumor-free region and embedded tumor. B) Loss of the top two waveguides when pressed on the tumor-free region and embedded tumor. C) Loss of the detection point (Bottom waveguide 1 and Top waveguide 1) and the resulting duty cycle signal.

palpation procedure based on feedback from clinicians. User trials would also help determine the optimal sensitivity of haptic feedback to provide to the surgeon.

CONCLUSION

This work describes an integrated palpation sensing and haptic feedback system for tumor detection in robotic-assisted palpation procedures. A soft optical palpation sensor is connected to a wearable haptic glove. The glove has multi-finger microfluidic actuators that inflate in response to tumor detection by the sensor. The sensor and the glove are made from easily available, cost-efficient materials including tubing and silicone. This allows quick fabrication of the sensor and glove and enables the sensor and actuators to be easily disposed of between procedures. The sensor is able to feel and localize the presence of tumors beneath the tissue phantom surface based on optical loss from its four waveguides. The sensor can detect the presence of tumors ranging from a depth of 2 mm to 5 mm beneath the surface of a tissue phantom. Concurrently, the sensor exhibits a downward trend in loss as the depth of the tumor increases. The actuators inflate proportionally to the loss encountered by the sensors via a PWM control algorithm to provide haptic feedback to a user (i.e., clinician). The system was able to be integrated with a Universal robot arm to perform a mock robotic palpation procedure (i.e., with a tissue phantom).

The next steps for this work would be to improve the resolution of the sensor, i.e., increasing the density of indenters and detection points. The sensor could also be improved to differentiate and quantify detecting tumors of different hardness. Lastly, the sensor circuitry could be further miniaturized to enable easy integration onto various robotic end effectors for palpation.

REFERENCES

- [1] K. H. Sheetz, J. Clafin, and J. B. Dimick, "Trends in the Adoption of Robotic Surgery for Common Surgical Procedures," *JAMA Network Open*, vol. 3, no. 1, 2020.
- [2] C. Tsui, R. Klein, and M. Garabrant, "Minimally invasive surgery: National trends in adoption and future directions for hospital strategy," *Surgical Endoscopy*, vol. 27, no. 7, pp. 2253–2257, 5 2013. [Online]. Available: <https://link.springer.com/article/10.1007/s00464-013-2973-9>
- [3] W. Othman, Z. H. A. Lai, C. Abril, J. S. Barajas-Gamboa, R. Corcelles, M. Kroh, and M. A. Qasaimieh, "Tactile Sensing for Minimally Invasive Surgery: Conventional Methods and Potential Emerging Tactile Technologies," *Frontiers in Robotics and AI*, vol. 8, p. 376, 1 2022.
- [4] L. Scimeca, J. Hughes, P. Maiolino, L. He, T. Nanayakkara, and F. Iida, "Action Augmentation of Tactile Perception for Soft-Body Palpation," *Soft Robotics*, vol. 9, no. 2, pp. 280–292, 4 2022.
- [5] N. Herzig, P. Maiolino, F. Iida, and T. Nanayakkara, "A Variable Stiffness Robotic Probe for Soft Tissue Palpation," *IEEE Robotics and Automation Letters*, vol. 3, no. 2, pp. 1168–1175, 4 2018.
- [6] L. Costi, P. Maiolino, and F. Iida, "Soft Morphing Interface for Tactile Feedback in Remote Palpation," in *2022 IEEE 5th International Conference on Soft Robotics, RoboSoft 2022*. Institute of Electrical and Electronics Engineers Inc., 2022, pp. 932–937.
- [7] C. Huang, Q. Wang, M. Zhao, C. Chen, S. Pan, and M. Yuan, "Tactile Perception Technologies and Their Applications in Minimally Invasive Surgery: A Review," *Frontiers in Physiology*, vol. 11, 12 2020.
- [8] L. Meli, C. Pacchierotti, and D. Prattichizzo, "Experimental evaluation of magnified haptic feedback for robot-assisted needle insertion and palpation," *The International Journal of Medical Robotics and Computer Assisted Surgery*, vol. 13, no. 4, p. e1809, 12 2017. [Online]. Available: <https://onlinelibrary.wiley.com/doi/full/10.1002/rcs.1809https://onlinelibrary.wiley.com/doi/abs/10.1002/rcs.1809https://onlinelibrary.wiley.com/doi/10.1002/rcs.1809>
- [9] A. Abiri, Y.-Y. Juo, A. Tao, Syed, J. Askari, J. Pensa, J. W. Bisley, E. P. Dutson, and W. S. Grundfest, "Artificial palpation in robotic surgery using haptic feedback," *Surgical Endoscopy*, vol. 33, pp. 1252–1259, 1234. [Online]. Available: <https://doi.org/10.1007/s00464-018-6405-8>
- [10] A. M. Okamura, "Haptic Feedback in Robot-Assisted Minimally Invasive Surgery," *Curr Opin Urol*, vol. 19, no. 1, pp. 102–107, 1 2009.
- [11] A. Abiri, J. Pensa, A. Tao, J. Ma, Y.-Y. Juo, S. J. Askari, J. Bisley, J. Rosen, E. P. Dutson, and W. S. Grundfest, "Multi-Modal Haptic Feedback for Grip Force Reduction in Robotic surgery." [Online]. Available: <https://doi.org/10.1038/s41598-019-40821-1>
- [12] L. Meli, C. Pacchierotti, and D. Prattichizzo, "Sensory subtraction in robot-assisted surgery: Fingertip skin deformation feedback to ensure safety and improve transparency in bimanual haptic interaction," *IEEE Transactions on Biomedical Engineering*, vol. 61, no. 4, pp. 1318–1327, 2014.
- [13] A. Gerald, R. Batliwala, J. Ye, P. Hsu, H. Aihara, and S. Russo, "A Soft Robotic Haptic Feedback Glove for Colonoscopy Procedures," in *2022 IEEE/RSJ International Conference on Intelligent Robots and Systems (IROS)*, Kyoto, 10 2022, pp. 583–590.
- [14] M. Zhou, D. B. Jones, S. D. Schwaizberg, and C. G. L. Cao, "Role of Haptic Feedback and Cognitive Load in Surgical Skill Acquisition," in *PROCEEDINGS of the HUMAN FACTORS AND ERGONOMICS SOCIETY 51st ANNUAL MEETING*, 2007, pp. 631–635.
- [15] M. Li, S. Luo, T. Nanayakkara, L. D. Seneviratne, P. Dasgupta, and K. Althoefer, "Multi-fingered haptic palpation using pneumatic feedback actuators," *Sensors and Actuators, A: Physical*, vol. 218, pp. 132–141, 10 2014.
- [16] G. Frediani and F. Carpi, "Tactile display of softness on fingertip," *Scientific Reports*, vol. 10, no. 20491, 2020. [Online]. Available: <https://doi.org/10.1038/s41598-020-77591-0>
- [17] A. Talasaz and R. V. Patel, "Remote palpation to localize tumors in robot-assisted minimally invasive approach," *Proceedings - IEEE International Conference on Robotics and Automation*, pp. 3719–3724, 2012.
- [18] C. Pacchierotti, S. Member, D. Prattichizzo, S. Member, and K. J. Kuchenbecker, "Cutaneous Feedback of Fingertip Deformation and Vibration for Palpation in Robotic Surgery; Cutaneous Feedback of Fingertip Deformation and Vibration for Palpation in Robotic Surgery," *IEEE TRANSACTIONS ON BIOMEDICAL ENGINEERING*, vol. 63, no. 2, 2016. [Online]. Available: <http://ieeexplore.ieee.org>.
- [19] A. Tzemanaki, G. A. Al, C. Melhuish, and S. Dogramadzi, "Design of a wearable fingertip haptic device for remote palpation: Characterisation and interface with a virtual environment," *Frontiers Robotics AI*, vol. 5, no. JUN, p. 62, 6 2018.
- [20] J. Guo, B. Xiao, and H. Ren, "Compensating Uncertainties in Force Sensing for Robotic-Assisted Palpation," *Applied Sciences* 2019, Vol. 9, Page 2573, vol. 9, no. 12, p. 2573, 6 2019. [Online]. Available: <https://www.mdpi.com/2076-3417/9/12/2573/htmhttps://www.mdpi.com/2076-3417/9/12/2573>
- [21] N. Bandari, J. Dargahi, and M. Packirisamy, "Tactile sensors for minimally invasive surgery: A review of the state-of-the-art, applications, and perspectives," pp. 7682–7708, 2020.
- [22] J.-H. Lee, Y. N. Kim, J. Ku, and H.-J. Park, "Optical-Based Artificial Palpation Sensors for Lesion Characterization," *Sensors*, vol. 13, pp. 11 097–11 113, 2013. [Online]. Available: www.mdpi.com/journal/sensorsArticle
- [23] H. Xie, H. Liu, L. D. Seneviratne, and K. Althoefer, "An optical tactile array probe head for tissue palpation during minimally invasive surgery," *IEEE Sensors Journal*, vol. 14, no. 9, pp. 3283–3291, 2014.
- [24] S. Mckinley, A. Garg, S. Sen, R. Kapadia, A. Murali, K. Nichols, S. Lim, S. Patil, P. Abbeel, A. M. Okamura, and K. Goldberg, "A Single-Use Haptic Palpation Probe for Locating Subcutaneous Blood Vessels in Robot-Assisted Minimally Invasive Surgery," in *2015 IEEE International Conference on Automation Science and Engineering (CASE)*, 2015, pp. 1151–1158. [Online]. Available: <http://cal-mr.berkeley.edu/>.